Journal of Alloys and Compounds 757 (2018) 87–97

Contents lists available at ScienceDirect

Journal of Alloys and Compounds

journal homepage: http://www.elsevier.com/locate/jalcom

Mechano-chemical synthesis, thermal stability and phase evolution in AlCoCrFeNiMn high entropy alloy

Vikas Shivam*, Joysurya Basu, Yagnesh Shadangi, Manish Kumar Singh, N.K. Mukhopadhyay

Department of Metallurgical Engineering, Indian Institute of Technology (BHU), Varanasi, 221005, India

ARTICLE INFO

Article history:
Received 9 March 2018
Received in revised form
4 May 2018
Accepted 5 May 2018
Available online 7 May 2018

Keywords:
Mechanical alloying
High entropy alloys
Thermal stability
Microstructure
Microwave sintering

ABSTRACT

An equiatomic AlCoCrFeNiMn hexanary high entropy alloy (HEA) was successfully synthesized by mechanical alloying. The 40 h milled powder exhibits chemical homogeneity with an average particle size of less than 3 μm. This alloy, after 40 h of milling produces a solid solution BCC phase ($a = 2.89 \pm 0.03$ Å), the lattice parameter of which is very close to the lattice parameter of Fe and Cr. Similar BCC solid solution phase is also obtained by following a two different milling schedule containing 3 elements i.e., AlCoCr & FeMnNi separately. Dynamic DSC thermogram of the hexanary alloy powder shows two exothermic peaks. The peak temperatures and heat evolution corresponding to each peak are sensitive to heating rates, indicating that the transformations are diffusional in nature. Phase evolution at these heat events was confirmed through high-temperature XRD and TEM study. It has been found that this alloy is stable upto 500 °C (773 K). Heat treatment at higher temperatures leads to the formation of a FCC phase closely related to Ni_3Al type and Mn_3Co_7 type intermetallic phase. Microwave sintered samples show the similar kind of behaviour as in heat-treated powder. The BCC phase along with ordered Ni_3Al type ($L1_2$) phase was observed in the bulk consolidated high entropy alloy. Thermo-physical properties of this alloy have been studied in order to elucidate its classification as high entropy alloy and to understand the essential differences with multicomponent glass forming alloys.

1. Introduction

The genesis of the new class of multi-component alloys in equiatomic or near equiatomic proportions of its constituents has opened up a new paradigm of materials engineering. There is a sudden upsurge of research in the scientific community to design and develop these alloys with the enhanced properties over the conventional materials [1–4]. It has been argued that pertaining to the multiple principal elemental composition, the high mixing entropy of these new alloys can overcome the enthalpies of the compound formation and leads to the formation of the simple disordered solid solution crystal structure of FCC, BCC or HCP [5]. The most generalized situation is that the free energy of the alloys will have a significant entropic contribution. The assumption of forming simple solid solution phase does not always hold good because there are only a few alloys which form single-phase solid solutions [6]. Equiatomic CoCrFeNiMn was the first alloy reported by Cantor et al. [2], which exhibited a single phase face-centered cubic (FCC) solid solution phase, although there are five elements and their crystal structures are different. Inspection of literature suggests that CoCrCuFeNi with a face-centered cubic (FCC) structure and AlCoCrFeNi with the body-centered cubic (BCC) structure are the most studied alloy systems. Wang et al. [7] have reported that in the AlCoCrFeNi alloy a body-centered cubic phase forms when prepared by vacuum arc melting technique. This alloy shows very interesting mechanical properties. Mohanty et al. [8] have reported the evolution of BCC and FCC phases after 60 h of mechanical milling of AlCoCrFeNi alloy and reported the phase separation after spark plasma sintering. Several hexanary additions of AlCoCrFeNi have been reported in the literature [9]. However, AlCoCrFeNiMn is worth mentioning as the phase formation and its stability are yet to be understood.

Various experimental techniques such as arc melting, injection casting, electrochemical deposition, mechanical alloying, melt spinning, laser cladding etc. have been used to prepare high entropy alloys (HEAs). Arc melting is one of the widely accepted

* Corresponding author.
E-mail address: vikas.rs.met13@itbhu.ac.in (V. Shivam).

https://doi.org/10.1016/j.jallcom.2018.05.057
0925-8388/

techniques to fabricate these alloys. However, segregation, as well as inhomogeneous microstructures, are the main drawbacks of this popular technique [10–12]. Mechanical alloying is one of the most promising techniques to produce a homogeneous microstructure with extended solid solubility among the elements [13,14]. Mechanical alloying followed by hot pressing and spark plasma sintering has been used most widely to synthesize bulk HEAs [15,16]. As densification is achieved by passing electric current for a short duration and soaking time is also limited, chances of segregation and microstructural changes are also restricted in this process [17]. HEAs synthesized by this technique have been reported to possess a combination of excellent properties, i.e. high strength and hardness. Apart from spark plasma sintering, microwave sintering is also an upcoming and viable technique for consolidation of high entropy alloy powders in the bulk form. In this sintering technique, the coupling of the microwaves with the dielectric proportion of the materials leads to the heat generation. Powder compacts directly absorb the microwave, and it is kept in SiC absorber, which acts as an auxiliary heat source. The volumetric heating ability of the microwave leads to the less processing time, and it is also energy saving [18–20].

High entropy alloys appear to have a few similarities & dissimilarities with the bulk metallic glass forming alloys. Number of components being the aspect of similitude; the composition selection criteria, nature of the enthalpies of mixing, atomic size mismatch etc. are the dissimilar factors. Akin to the glass forming alloys, understanding the thermodynamic criteria for high entropy alloy formation remains to be a major challenge. Even though there has been a considerable effort, a unified picture is still illusive. In addition to that, the phase and microstructural evolution and its stability over temperature-time space are the important aspects to be understood as this would eventually play an important role for application of these alloys [21]. In this light, in the present work, AlCoCrFeNiMn hexanary alloy has been synthesized by mechanical alloying followed by microwave sintering. The phase, microstructure and its stability have been studied by X-ray diffraction, electron microscopy and differential scanning calorimetry. Finally, an attempt has been made to advance our understanding of synthesis and stability of this alloy system.

2. Materials and experimental details

High purity (>99 wt%) elemental powders of Al, Co, Cr, Fe, Ni, and Mn with particle size ≤ 325 mesh were used as the starting materials. These powders were mixed in the equiatomic proportion at room temperature and then milled in a high-energy planetary ball mill (Retsch PM 400) using tungsten carbide (WC) vials and balls of 10 mm diameter with the rotation speed of 200 rpm. Milling was carried out in the wet atmosphere upto 40 h using toluene as the process control agent with a ball to powder weight ratio of 10:1. Milled powders were extracted at a regular interval of 5 h and were characterized to understand the milling behaviour.

Structural and microstructural characterizations were carried out by X-ray diffraction (XRD), (Rigaku Mini flex-600 (40 kV-15 mA)) and high-temperature XRD by Rigaku Smart Lab (45kV-200mA) with Cu-Kα radiation (λ = 0.154 nm), scanning electron microscopy (SEM), (FEI Quanta 200 F) operating at 20 kV, transmission electron microscopy (TEM TECHNAI G^2 T20) operated at 200 kV and optical microscopy (Metalux-3). Thermal analysis of 40 h milled powder was performed by using NETZSCH DSC 404 F apparatus in a nitrogen atmosphere at four constant heating rates of 10, 20, 40 & 50 K/min. For heat treatment of the powder, samples were vacuum sealed in the quartz tube to avoid oxidation. Subsequently, milled powders of 40 h, were consolidated in the form of green pellets of 10 mm diameter with 637 MPa normal pressure by using 30 ton capacity press. These green pellets were then sintered in the microwave furnace (with frequency of 2.45 GHz and power 3 kW) at three different temperatures of 900 °C (1173 K), 950 °C (1223 K) and 1000 °C (1273 K) respectively for 1 h followed by furnace cooling.

3. Results

Fig. 1 shows the multiple display of X-ray diffraction patterns of AlCoCrFeNiMn high entropy alloy powders after different milling hours. The diffraction peaks corresponding to all alloying elements can be predominantly observed in the initial blending of the powders i. e. after 10 min of milling. After 5 h of milling, diffraction intensities for all the elements decreases and the peaks tend to broaden. The intensity of the peaks corresponding to (111) plane of Al (d~2.32 Å), (311) plane of Al and (220) plane of Mn (d~1.21 Å) are reduced significantly after 5 h of milling. It has been found that diffraction peaks corresponding to Al disappear earlier than the other elements. Further increase in milling time upto 10 h suggests that most of the peaks, lose their identity except Mn. This indicates that the formation of a solid solution by dissolution of most of the element in the lattice of Fe or Cr. The identification of the host lattice is not quite straightforward at this stage but it is close to Fe & Cr. By increasing the milling time for next 5 h, it can be observed that there is no change in the peaks position. However, the peaks can clearly be indexed to a BCC lattice. Milling upto 20 h and afterwards indicates the formation of the same cubic phase, the lattice parameter of which is higher than Fe but lower than Cr. The lattice parameter, as measured from the XRD pattern, turns out to be ($a = 2.89 \pm 0.02$ Å). This indication becomes increasingly evident on further increasing in milling time up to 30 h. The XRD pattern of the 30 h milled powder has a strong agreement with a solid

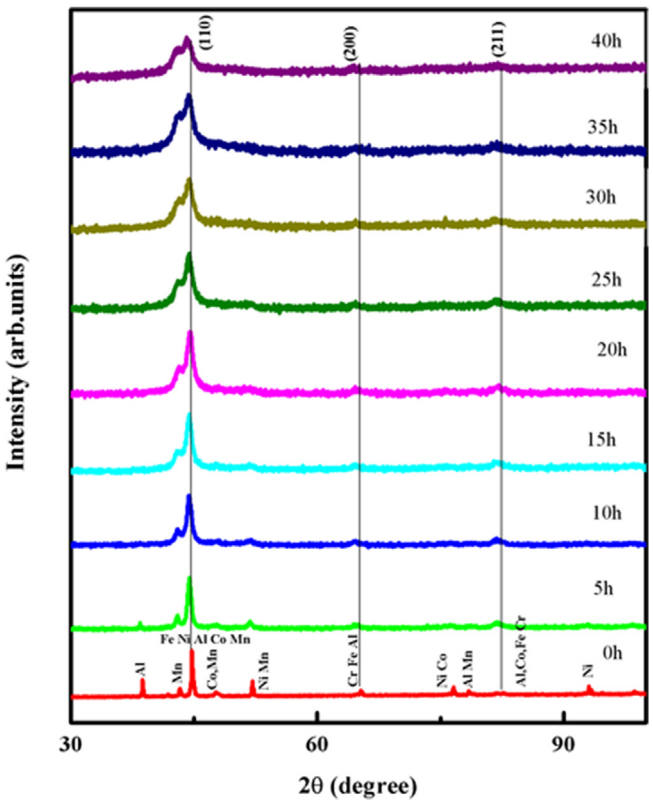

Fig. 1. XRD patterns of AlCoCrFeNiMn HEA powders with different milling time. Evolution of the BCC phase is evident with the progress of milling.

solution phase with BCC structure. While analyzing the diffraction patterns with milling time, it has been found that the intensity decreases and broadening of the peaks takes place. This was expected because the increase of milling time decreases the crystallize size and increases the lattice strain, which are reported in Table 1. This increase in lattice strain is mainly due to the introduction of elements in the host lattice of the high entropy alloy and mechanical working of the powder during the mechanical alloying process. Although the complete solid solution was found to have formed at 30 h of milling time, still milling was continued upto 40 h in order to investigate any further phase transformation. However, no phase transformation could be detected. Hence it is clear that 40 h milled powder shows the formation of a single-phase solid solution of BCC structure with lattice parameter ($a = 2.89 \pm 0.03$ Å). This solid solution formation may be the result of the high entropy effect of the alloying elements because all the alloying elements are in the equiatomic proportions. Here it is worthy to note that in AlCoCrFeNiMn high entropy alloy system two elements (Fe, Cr) are having simple BCC structure and two (Al, Ni) having FCC along with one (Co) hexagonal structure(HCP). It may be mentioned that Mn is having a complex BCC structure similar to γ-brass structure. It is important to emphasize that the final high entropy alloy phase is a simple BCC in structure of Fe, Cr type. It may appear that the phase selection of high entropy alloy could be driven by the structure of maximum number of constituent elements of high melting temperature. However, it may not be often always true. Wang et al. [22] have reported that Al stabilizes the FCC structure when it is less than 11 at%, and it enhances the formation of BCC structure when it is present in more amount. From the lattice parameter of the BCC phase, it can be assumed that the lattice of Fe is acting as the host lattice for this alloy system and the lattice parameter is slightly more than that Fe and less than that of Cr. This result is also along the line of Hume-Rothery rule of solid solution formation, which restricts the atomic radii difference between two constituent elements below 15%. In AlCoCrFeNiMn high entropy alloy atomic size difference of elements is not more than 8% what is desired for solid solution formation.

In order to understand the mechanism of solid solution phase formation, this hexanary alloy system was divided into two (ternary) alloy systems. These alloy systems were taken on the basis of their milling behaviour during the hexanary alloy. AlCoCr and FeMnNi systems were separately milled upto 20 h and their milling behaviour with time was followed by XRD. After that 20 h, milled powder from both the ternary alloys were mixed together and they were milled for another 20 h to observe the final phase formation. The evolution of phases in AlCoCr alloy system upto 20 h of milling as followed by XRD is given in Fig. 2a. From this figure, all the elemental peaks of Al, Co & Cr are observed after 10 min of milling. However, with further milling initially Co peaks disappear, and the peaks get broadened due to the refinement of particle size and the introduction of strain. With further milling, some of the major peaks of Al also disappear finally leading to the formation of a BCC phase after 20 h of milling. Milling behaviour of FeMnNi ternary alloy as followed by XRD is given in Fig. 2 (b). In this system also individual elemental peaks of Fe, Ni and Mn are observed in the XRD pattern after 10 min of milling. In this alloy system, Mn peaks

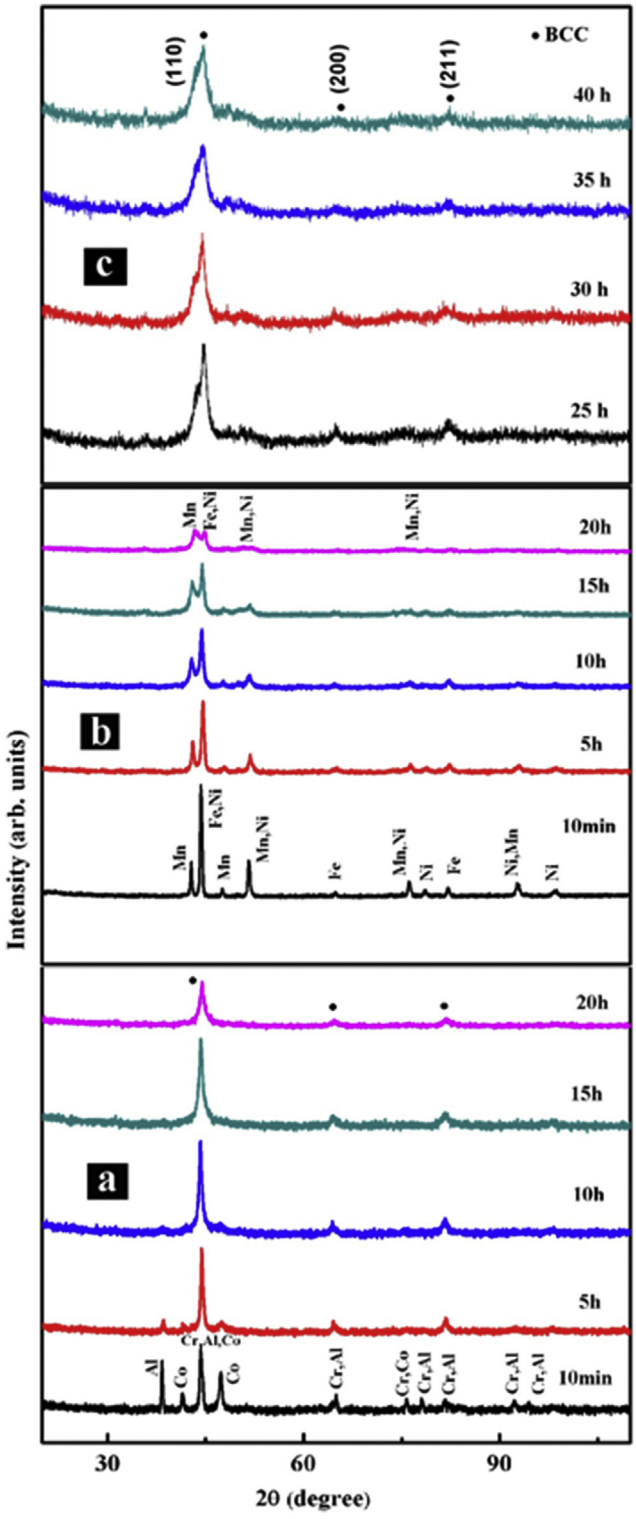

Fig. 2. XRD patterns of (a) AlCoCr (b) FeMnNi (c) AlCoCrFeNiMn HEA powders with different milling time. In (a) after 20 h of milling, no known phase appears. In (b) the phases cannot be ascertained and in (c) BCC phase appears after 25 h of milling of 20 h milled powder of (a) & (b).

Table 1
The crystallite size and lattice strain of equiatomic AlCoCrFeNiMn high entropy alloy powder.

Milling time (h)	5 h	10 h	15 h	20 h	25 h	30 h	35 h	40 h
Crystallite size (nm)	20	18	17	17	16	15	15	15
Lattice strain (%)	0.54	0.61	0.63	0.66	0.67	0.68	0.69	0.70

are the first to disappear or lose their identity. This necessarily means that Mn dissolves into another lattice first. Subsequently, some of the major peaks of Ni disappear and finally after 20 h of milling a phase evolves, the structure of which could not be

ascertained. The phase evolution of mixed milled powder from the above two sets over next 20 h as followed by XRD is shown in Fig. 2c. As observed from the XRD patterns, 5 h of milling of the mixed powder leads to the formation of the BCC phase. Further milling does not lead to any change in the phase structure. However, the broadening of the peaks is evident. So from this study, it can be concluded that although mechanical alloying is a non-equilibrium process, similar phase evolves after different milling sequence. It appears that phase evolution in this particular alloy system becomes path independent in the long run.

Morphology of 40 h milled alloy powder is given in Fig. 3. It is observed that the particles are irregular in shape and their size varies in the range of 1–10 μm. Very often river like flow patterns are observed on the particle surfaces, which have arisen due to the shear type of deformation and fracturing of the particles during the milling process. Size distribution of particles in the alloy is in the micron range and plot of this has been shown in Fig. 4. In doing the particle size measurement, absolute measurement technique was adopted, i.e. the particle size was measured directly from the micrograph and the largest dimension was taken as the particle size.

The presence of the phases and their alloying effects were investigated in detailed manner through the transmission electron microscopy. Bright field images, and corresponding SAD patterns have been shown in Fig. 5 (a) and 5 (b) respectively. The formation of ring patterns in the SAD pattern indicates the alloy particles are randomly oriented. Indexing of these ring patterns confirms that a single BCC phase ($a = 2.91 \pm 0.02$ Å) is present in the 40 h milled AlCoCrFeNiMn high entropy alloy powder. Additionally, the d-spacings corresponding to these rings are matching closely with those observed in the X-ray diffraction patterns. There are two intense spots in the SAD pattern corresponding to 2.36 Å. It does not match with any known d-spacing of any of the constituent elements, neither this peak was observed in X-ray diffraction pattern. A careful investigation reveals that this d-spacing corresponds to Cr_2O_3 (110) and Al_2O_3(110). Fig. 5 (c) shows the high-resolution image (HRTEM) of the 40 h milled high entropy alloy powder. In the image, lattice fringes corresponding to the alloy is observed in multiple directions. The random orientation of the particles and lattice fringes further confirms the origin of regular ring pattern in the diffraction pattern. In addition to that, the particles are faceted, might have originated from the fracturing of the particles during mechanical alloying. Due to the presence of different elements in the lattice, the lattice planes are expected to be distorted. The lattice fringe corresponding to the oxide is also observed in the high-resolution image. The regions where lattice fringes are disappearing are the regions where fracturing took place, and it is along a definite plane due to the huge amount of micro strain present in the alloy. This large amount of micro strain is due to the mechanical alloying and addition of elements in the high entropy alloys. Interplanar spacing from these lattice fringes is 2.36 Å which closely matches with the Cr_2O_3(110), and 2.11 Å corresponds to the BCC phase of (110) plane.

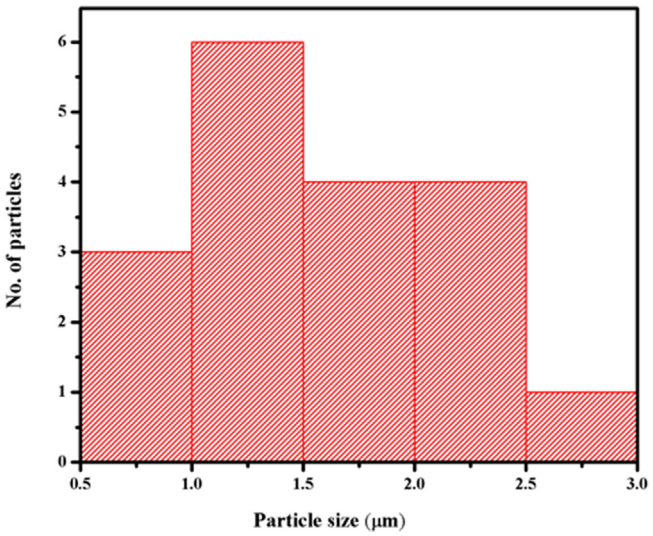

Fig. 4. Particle size distribution in equiatomic AlCoCrFeNiMn high entropy alloy after 40 h of milling. The median particle size is in the range ~ 1–1.5 μm.

The STEM-EDS elemental mapping of the 40 h milled powder sample has been shown in Fig. 6. It has been found from the elemental mapping that all the elements of the hexanary alloy are distributed uniformly. There is no signature of heterogeneity. This confirms that all the constituent elements are incorporated in the host lattice to give rise to the high entropy alloy. However, a detailed look at the elemental maps indicates that a minor variation in intensity is present in the maps. As the alloyed particles are repeatedly fractured, their shapes are not uniform and considerable variation in thickness also exists. Pertaining to these two factors, interaction volume of the electron beam with the particles changes and X-ray signal generation undergoes changes locally, which might have led to the variation in intensity.

Thermal stability of the 40 h milled high entropy alloy has been investigated through dynamic DSC at different heating rates (10, 20, 40 & 50 K/min) and corresponding thermograms are shown in Fig. 7. Eventhough, similar thermal events are seen in all the thermograms, their intensity varies. At the higher heating rate, two exothermic heat events are observed. However, at a lower heating rate, and the higher temperature heat event is absent. Additionally,

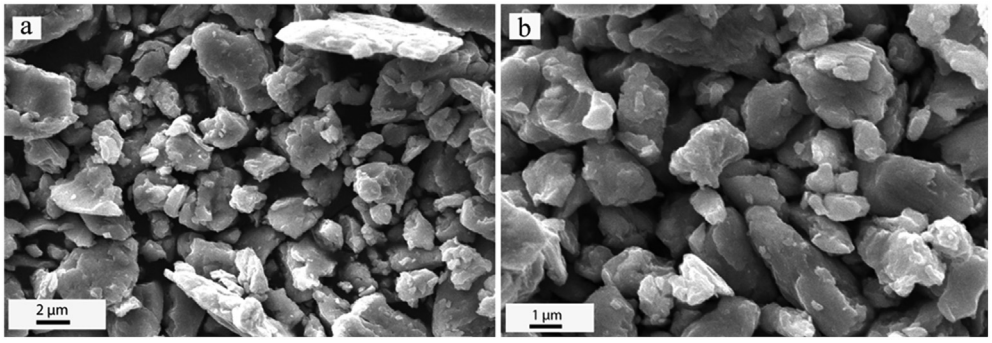

Fig. 3. SEM micrographs of AlCoCrFeNiMn HEA powders with 40 h of milling at different magnifications. In both the cases fractured particles with extensive river pattern on the surfaces can be observed.

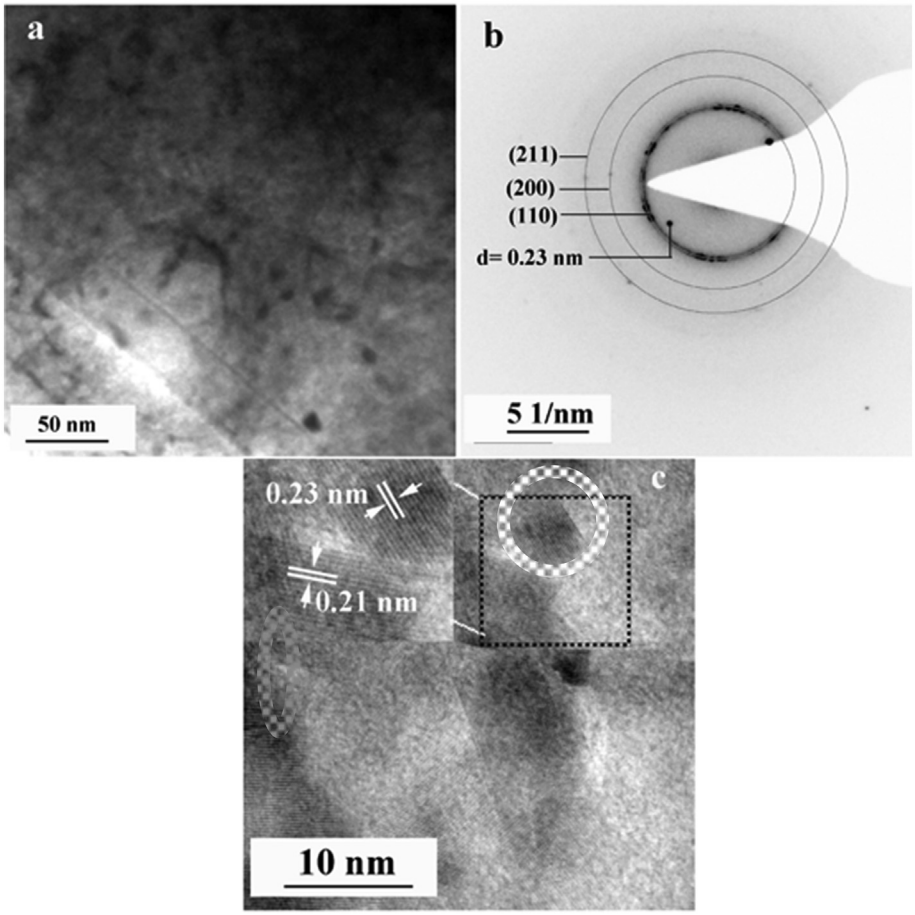

Fig. 5. TEM bright field image (a) of 40 h milled AlCoCrFeNiMn HEA powder and corresponding SAD pattern (b) with HRTEM (c). From the diffraction pattern, the presence of the BCC phase can be confirmed. Similar spacings are observed in the high-resolution image also.

the intensity of the first heat event (exothermic in nature) decreases with the decrease in the heating rate. This is due to the fact that the transformations corresponding to these heat events are diffusive in nature and they are not so sensitive to the characteristic temperature. At lower heating rate as long incubation or residence time is available, the transformation starts at lower temperature itself, which leads to the reduction in heat evolution at the characteristic temperature. In a similar line, it could be argued as to why the higher temperature heat events are missing in the thermograms with lower heating rates. With higher heating rates, due to the unavailability of enough residence time, the heat events are much more pronounced. It is important to mention that the heat events at higher heating rates gradually transfer to the higher temperature side due to the diffusive nature of the transformation processes. The second heat event that appears at 40 K/min heating rate is not so clearly visible at 50 K/min heating rate, probably due to its shift to a higher temperature. However, the transformation related to this heat event is real that is confirmed by ex-situ heat treatment and subsequent structural characterization, which has been reported in the following sections.

Activation energy calculation for the transformation of this alloy has been done through Kissinger and Ozawa models [23,24]. Plots were drawn using these equations:-

$$\ln\left(\frac{\beta}{T_p^2}\right) = -\frac{E}{RT_p} + C_1 (\text{Kissinger equation}) \quad (1)$$

$$\ln(\beta) = -\frac{E}{RT_p} + C_1 (\text{Ozawa equation}) \quad (2)$$

From the slope and the intercept of the straight line, it is possible to calculate the activation energy of transformation for both the equations. Here β is the heating rate in K/min, T_p is the peak temperature (Kelvin), R is the universal gas constant and E is the activation energy. All the relevant data and activation energies have been shown in Table 2. The activation energy of the second heat event was not possible to be calculated as the peak was not observed at lower heating rates. The activation energies for the first heat event by Kissinger method and by Ozawa method turn out to be 310 and 324 kJ/mol respectively. Given the assumptions of these models, the values are quite close and corroborating.

In order to understand the phase transformations associated with the heat events as observed in DSC, high-temperature in-situ XRD was conducted of this 40 h milled powder sample at seven different temperatures form 350 °C (623 K) to 800 °C (1073 K) at regular interval of 75 °C (346 K). XRD patterns as obtained at all these temperatures have been shown in Figs. 8 and 9. Fig. 8 consists of the X-ray diffraction patterns as obtained upto 500 °C (773 K) and Fig. 9 consists of the patterns as obtained above 500 °C (773 K). From XRD plot, it can be seen that there was no change in the phase

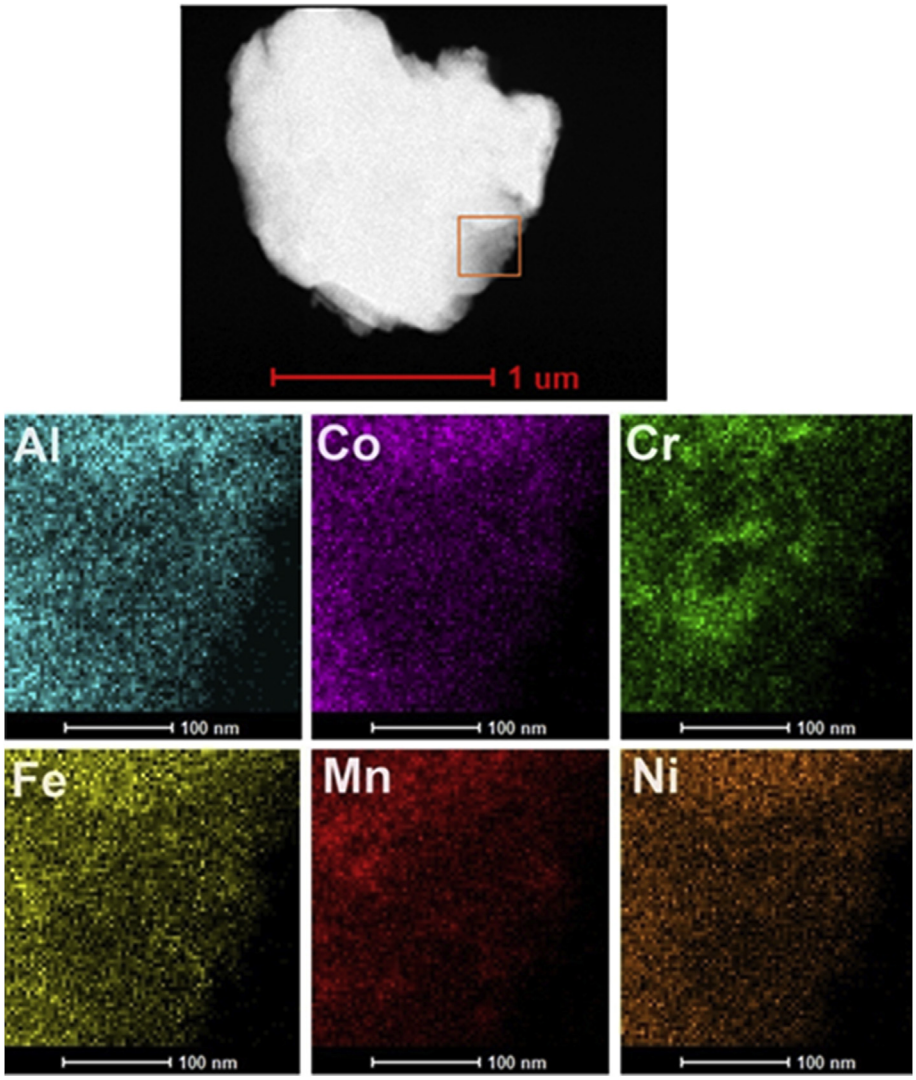

Fig. 6. The STEM-EDS mapping of equiatomic AlCoCrFeNiMn hexanary high entropy alloy after 40 h of milling. The elements are homogeneously distributed to give rise to the single BCC phase.

upto 500 °C (773 K), it means that this alloy is stable upto this temperature for the said interval of time. Detailed analysis of the peak positions of all the XRD patterns has been done. It has been found that at 575 °C (K) nucleation of Mn_3Co_7 and $L1_2$ type (Ni_3Al type) phase along with the retained BCC phase takes place. Further analysis of the diffraction patterns corroborates these phenomena in the same line upto 650 °C (923 K). It is interesting to observe that at 725 °C (998 K) a FCC phase appears along with the other retained phases. This FCC phase ($a = 3.63 \pm 0.02$ Å) also has a strong proximity with $L1_2$ type (Ni_3Al type ($a = 3.67 \pm 0.03$ Å)) phase. It has been observed from the thermal stability study and nature of phase evolution that the transformation through which the alloy changes its phase constituent and microstructure is diffusive in nature. Pertaining to this behaviour, it is difficult to assign a singular and accurate temperature for thermal stability. The thermal stability temperature quoted above should be taken as a ballpark value. In the X-ray diffraction pattern after heat treatment at 500 °C, small peaks of the second phase could be observed. The intensity of those peaks being small it has been considered that the volume fraction of those phases is relatively small to introduce any significant change in the microstructure.

To understand thermal stability, the high entropy alloy samples annealed at 500 °C (773 K) and 800 °C (1073 K) were observed in TEM. Bright field images with corresponding diffraction patterns of these samples have been shown in Figs. 10 and 11. The bright field image of the alloy heat-treated at 500 °C (773 K) (Fig. 10) reveals the fine-grained structure of the alloy in which grains are irregular in shape, and their size ranges between 5 and 10 nm. In the diffraction pattern the rings corresponding to the BCC phase is obtained. This further proves that the alloy is thermally stable upto 500 °C (773 K). The bright field image of the alloy after heat treatment at 800 °C (1073 K) (Fig. 11) shows two types of polygonal grains, which are basically different in their size. One type of grains, which are mostly distributed all over the matrix are in size range of 50–100 nm. The other type of grains, which is scattered in the matrix, is in size range of 15–30 nm. In the diffraction patterns, the signature of BCC phase, as well as FCC phase, could be ascertained.

Visible light micrographs of microwave sintered AlCoCrFeNiMn high entropy alloy, which were sintered at 900 °C (1173 K), 950 °C (1223 K) & 1000 °C (1273 K) are shown in Fig. 12. From micrographs, it can be seen that as the temperature of sintering increases coarsening of the grains increases. In the same line porosity (shown with arrow) of the sample decreases which can also be observed. XRD patterns of the alloy microwave sintered at 900 °C (1173 K),

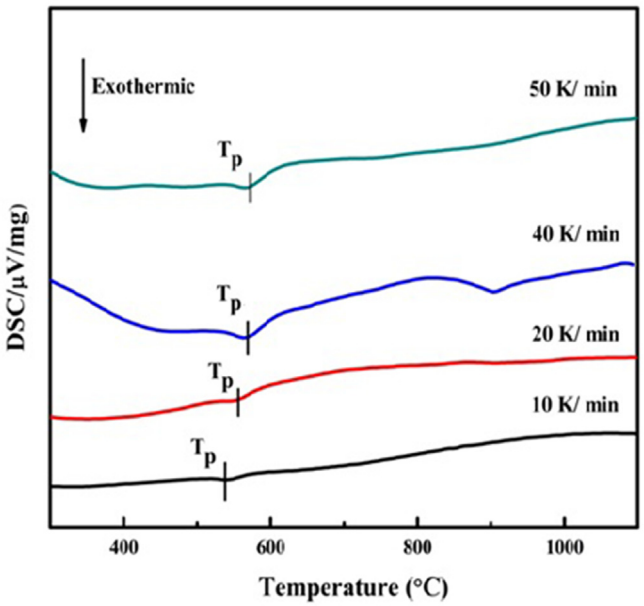

Fig. 7. DSC thermogram of 40 h milled AlCoCrFeNiMn high entropy alloy powder at different heating rates. Two exothermic heat events are observed at higher heating rates which are reduced to one heat event at lower heating rates, attributed to the diffusional nature of the transformation process.

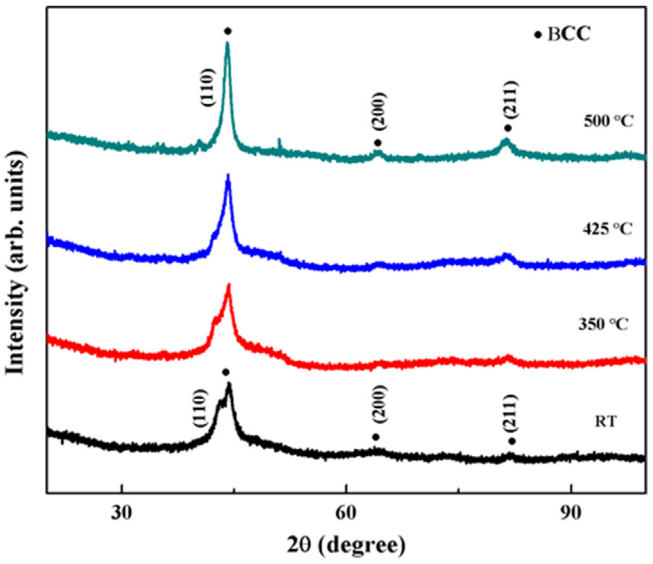

Fig. 8. XRD patterns of 40 h milled AlCoCrFeNiMn high entropy alloy powder upto 500 °C (773 K). No phase transformation is observed up to this temperature, which signifies that the alloy is stable up to this temperature.

950 ° C (1223 K) & 1000 °C (1273 K) have been shown in Fig. 13. It is evident that along with the BCC phase, the nucleation of an ordered Ni_3Al type intermetallic phase takes place.

4. Discussion

4.1. HEAs and BMGs

The discovery of high entropy alloys began almost at the same time as that of bulk metallic glass forming alloys [1]. However, scientific community took serious interest in exploring and understanding the nuances of alloy design in this category little more than a decade later [3]. A peek into the alloy design strategies for high entropy alloys reveals that there are quite a few similarities in these two alloy systems [25]. For bulk metallic glass formation the atomic size difference is prescribed to be more than 15% leading to structural frustration in the crystal which is just the opposite to what has been prescribed for high entropy alloys. In case of high entropy alloys, the atomic size difference less than 15% basically favours substitutional solid solution formation. While the atomic size mismatch criteria for bulk metallic glass formation may be considered as opposite to Hume-Rothery rule for solid solution formation, the same for high entropy alloys may be seen as pro Hume-Rothery rule. The atomic size difference among all the elements of AlCoCrFeMnNi alloy is given in Table 3. It is observed that none of the differences is above 15%. The second level of difference that exists is the restriction on composition in case of high entropy alloys. It is recommended to be within 5–35 at%. No such guideline

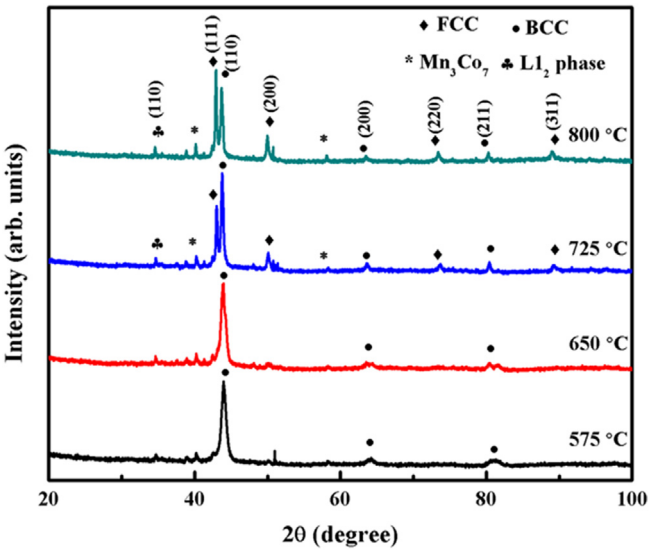

Fig. 9. XRD pattern 40 h milled AlCoCrFeNiMn high entropy alloy powder upto 800 °C (1073 K). Sequential precipitation of $L1_2$ phase and Mn_3Co_7 phases are clearly observed.

exists for bulk metallic glass forming alloys. However, bulk metallic glasses with equiatomic or almost equiatomic composition has been reported in the literature [26]. Additionally, for bulk metallic glasses, it has been recommended that the binary enthalpies of mixing should be highly negative that favours intermetallic phase formation. In stark contrast to that, it has been reported that in high

Table 2
Activation energy calculation by Kissinger and Ozawa model for the first transformation event of the AlCoCrFeNiMn high entropy alloy.

Heating Rate (β), K/min	Peak Temperature (K)	Activation Energies kJ/mol-K	
10	814	310 (Kissinger model)	324 (Ozawa model)
20	822		
40	838		
50	840		

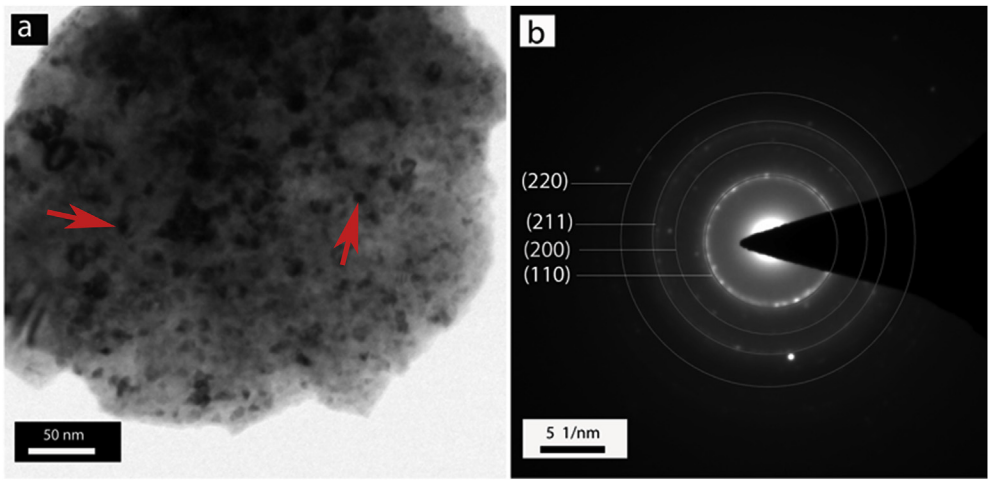

Fig. 10. Bright field image and corresponding SADP of AlCoCrFeNiMn powder sintered at 500 °C (773 K) under control atmosphere. Fine-grained structure (shown with arrows) of the alloy and the presence of the BCC phase is observed after sintering.

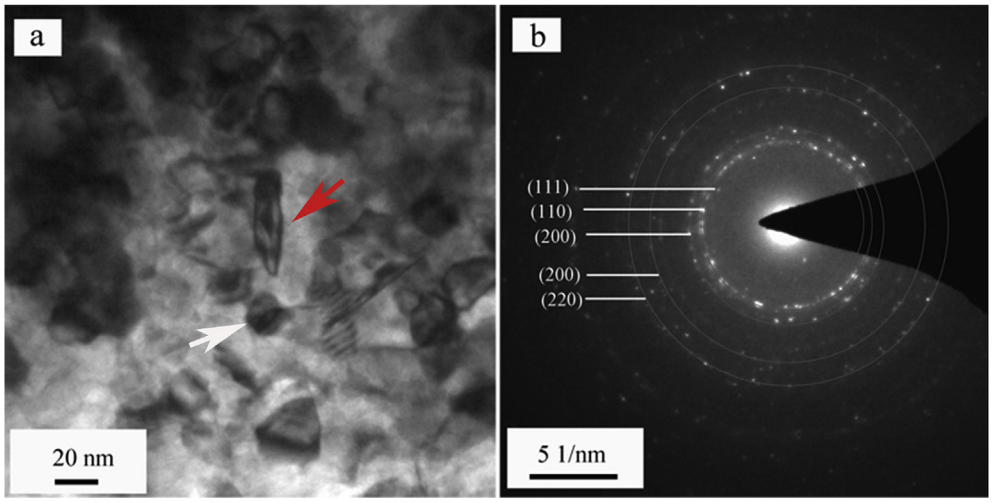

Fig. 11. (a) Bright field image and (b) corresponding SADP of AlCoCrFeNiMn powder sintered at 800 °C (1073 K) under control atmosphere. The grains are faceted (shown with arrows) however not extraordinarily grown due to sluggish diffusion kinetics.

entropy alloys, entropy of mixing should play an important role. Hence entropy should be considered in order to assess the stability and formation of high entropy alloys. As intermetallic based high entropy alloys have also been reported, it is a challenge to establish semiempirical thermodynamic criteria to predict the stability of high entropy alloys. In a remarkable advancement in that direction, Zhang et al. [27] have reported that the ratio between $T\Delta S_{mix}$ and ΔH_{mix} should be taken into consideration. They have shown that in the ratio of high entropy alloy forming systems it is always more than one whereas the same for the bulk metallic glass forming alloys is less than 1. The binary heats of mixing of several components in AlCoCrFeNiMn are given in Table 4. These binary enthalpy of mixing are calculated on the basis of Miedema macroscopic model [28]. It is observed from the table that none of the binary heats of mixing is positive which necessarily indicates that there should not be any likely tendency for phase separation. Moreover, the heats of mixing values are negative however small. The only high negative enthalpy of mixing is observed in Al-Ni, Al-Co and Al-Mn systems, which are reported in Table 4. In these systems, quite a few intermetallic phases are observed. Basu and Ranganathan [29] earlier reported through a series of phase diagram search that number of intermetallic phases are somehow empirically related to the heat of mixing. This alloy system is also not an exception to that. For the present alloy system T_m, ΔS_{mix} and ΔH_{mix} are calculated and reported in Table 5. It has been observed that the ratio as proposed by Zhang et al. turns out to be 2.5 for this alloy system. This is very much in the range as proposed in the earlier literature. The discussion above brings out clearly the difference of this alloy system with bulk metallic glass forming alloys and its suitability as a high entropy alloy.

4.2. Mechanical alloying behaviour of AlCoCrFeMnNi HEA

In the present work, the alloy system was mechanically milled, and the evolution of phases was monitored with a specific time interval. It has been observed that the Al, Co and Mn peaks disappear sequentially. It has been understood that the elements with lower melting point lose their identity first [30]. In the present case Al along with Co & Mn gets dissolved and Fe, Cr retains its identity. Based on this observation, it can be concluded that the melting point criteria might be system specific or at least does not hold good universally. Further authors would like to note that

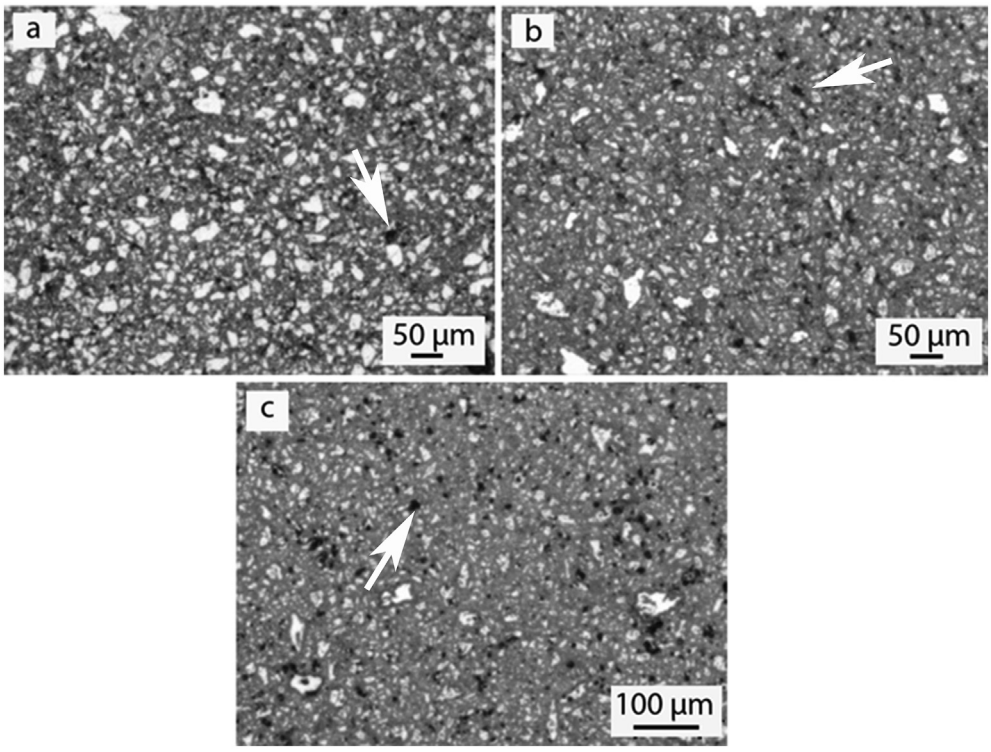

Fig. 12. Optical micrographs of AlCoCrFeNiMn HEA compact after microwave sintering at (a) 900 °C (1173 K) (b) 950 °C (1223 K) (c) 1000 °C (1273 K). Fine distribution of grains and porosity (shown with arrows) can be observed.

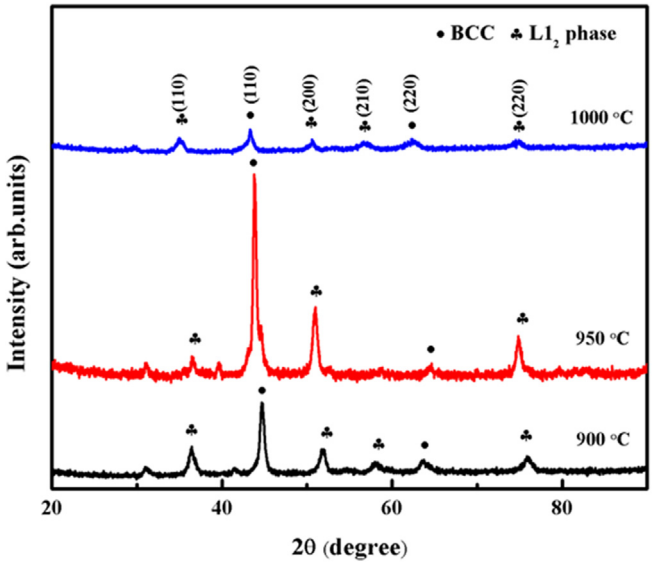

Fig. 13. XRD patterns of AlCoCrFeNiMn HEA alloy compact after microwave sintering at 900 °C(1173 K), 950 °C (1223 K) & 1000 °C (1273 K). Along with the BCC phase, the presence of $L1_2$ phase can also be discerned.

dissolution criteria based on melting point is partially based on empiricism and there are other factors, which might change the dissolution behaviour. Moreover, disappearance or reduction of intensity of certain peaks of an element in XRD may be the effect of various other factors relating to the scattering behaviour of that particular element. A definitive conclusion needs further work and close sensitivity of the milling behaviour. This issue is worth pursuing for better understanding. As the milling time increases peaks

Table 3
The values of atomic size difference δ (%) in the AlCoCrFeNiMn high entropy alloys system.

Element	Al	Co	Cr	Fe	Ni	Mn
Al	–	6.7	6.8	7.1	6.9	2.9
Co	6.7	–	0.08	0.4	0.2	3.8
Cr	6.8	0.08	–	0.32	0.12	3.9
Fe	7.1	0.4	0.32	–	0.20	4.2
Ni	6.9	0.2	0.12	0.20	–	4.0
Mn	2.9	3.8	3.9	4.2	4.0	–

intensity decreases with increase in broadening. This is expected because the increase in milling time decreases the crystallite size and increases the lattice strain. The complete formation of the solid solution phase has been found after the 30 h of milling. Milling was further increased upto 40 h to investigate any phase transformation, but it does not exhibit any change. The earlier report shows that similar phases are present even after 60 h of milling [9]. This necessarily means that after 30 h of milling no further change in the structure of this alloy takes place and this excess hour of milling is basically redundant so far the phase evolution in this alloy is concerned. The 40 h milled sample showed the single-phase solid solution of BCC crystal structure, which was confirmed through XRD and TEM study. In an earlier study, it has been reported that a FCC phase along with the BCC phase appears after completion of milling though in minor quantities. In the present case, rigorous analysis of the diffraction patterns does not confirm presence of FCC phase which has been reported by Wang et al. [9], and this difference in observation could be attributed to different milling condition. High-resolution phase contrast images from the milled powder reveals the lattice structure of the BCC phase. The lattice plane corresponding to the BCC phase has also been resolved. However, occasionally a lattice fringe has been resolved

Table 4
The values of chemical enthalpy of mixing(ΔH_{ij}^{mix}, kJ/mol), of atomic pairs for AlCoCrFeMnNi high entropy alloy, following the Miedema's approach [28].

Element	Al	Co	Cr	Fe	Ni	Mn
Al	–	−19	−10	−11	−22	−19
Co	−19	–	−4	−1	0	−5
Cr	−10	−4	–	−1	−7	2
Fe	−11	−1	−1	–	−2	0
Ni	−22	0	−7	−2	–	−8
Mn	−19	−5	2	0	−8	–

Table 5
Calculated thermodynamic and physical parameters for AlCoCrFeMnNi high entropy alloy.

ΔH_{mix} $\left(KJ/mol\right)$	T_m (K)	ΔS_{conf} $\left(\frac{JK^{-1}}{mol}\right)$	Ω
−11.39	1944	14.89	2.5

which does not match with the BCC phase. The fringe spacings match with the oxide of aluminium. As the milling was carried out in an inert atmosphere, the possibility of forming oxide phase even in minor quantities can not be ruled out. However, the powder was dried in air, which could have resulted in minor oxide phase formation. In any case, this cannot be related to the phase structure of the alloy. In a similar line, carbide formation has been reported in wet milling and/or after subsequent heat treatment. In case of carbide formation, corresponding diffraction peaks are observed in X-ray and electron diffraction patterns. Moreover, predominant contrast enhancement in STEM-EDS maps is also observed in localized regions. In the present study, none of the above-mentioned features could be observed, which rules out the possibility of extended carbon contamination and carbide formation [31]. In order to further understand the solid solution phase formation mechanism of this hexanary alloys, the alloy was divided in two ternary alloy systems. These two ternary alloy systems (AlCoCr and FeMnNi) were milled for upto 20 h in the separate vials. After the 20 h of milling these two systems were mixed together and mixed powder was milled for further 20 h. This new way of milling of high entropy alloy system shows the same phase as was found in the single hexanary alloys system. From this study, it can be deduced that although the mechanical alloying is the non-equilibrium process but it evolves the same phase and independent of the processing route for this particular alloy system.

4.3. Thermal stability of the phases evolved in the AlCoCrFeMnNi HEA

In the dynamic differential scanning calorimetric thermogram, it has been observed that phase composition of the alloy changes in two separate exothermic heat events when it is heated upto 1100 °C (1373 K). The alloy is stable upto 500 °C(773 K), and subsequently, the heat events appear at around 540 °C(813 K) and 900 °C (1173 K). It is important to note that the peak temperatures for these heat events shift to the right as the heating rate is increased. In addition to that, the heat evolved at each event is increased as the heating rate is increased. These observations can be explained in the light of diffusional transformation. Similar behaviour is observed in the glasses and other metastable alloys when they undergo diffusional transformation [32,33]. As the diffusional transformation has a characteristics incubation time as the heating rate increases the peak shifts to the higher temperature side. Moreover, at lower heating rates as more of residence time is available, the diffusional transformation starts beforehand leading to a decrease in the heat evolution at the peak temperature. The activation energies calculated based on two different models corroborate well. Though published literature does not exist on this particular transformation, activation energies for transformation in glasses and metastable alloys lie in this range only.

The phases evolved with the heat events have been explored through in-situ high-temperature XRD and TEM. It is observed that a FCC phase, which is quite closely related to the Ni_3Al phase, evolves after the first transformation event. After the second transformation, Mn_3Co_7 phase could be observed in the alloy. The evolution of this phase after heat treatment has been reported in the earlier literature [9]. As a result of the evolution of these phases, the high entropy alloy matrix should become richer in the remaining elements. Transmission electron microscopy reveals that the phases are nanocrystalline. It is likely to happen as the alloy is multicomponent, the diffusion of the elements leading to the transformation is likely to be sluggish. Similar, phase evolution has been observed after sintering also.

5. Conclusions

It can be concluded from the present work that

1. AlCoCrFeNiMn equiatomic alloy leads to the formation of a single-phase BCC ($a = 2.89 \pm 0.03$ Å), alloy upon mechanical alloying. Similar phase evolution is obtained by dividing the alloy composition into two different segments and milling them in a different schedule.
2. The semi-empirical thermodynamic analysis reveals that the ratio of TΔS/ΔH is ~2.5 which is well within the range of high entropy alloys as reported in the literature.
3. The high entropy alloy is stable upto ~500 °C (773 K), and then it undergoes two diffusional transformations leading to the precipitation of a nanocrystalline FCC ordered phase ($a = 3.63 \pm 0.02$ Å) closely related to Ni_3Al type intermetallic phase with subsequent precipitation of Mn_3Co_7 phase.
4. Consolidated and sintered pellet of the same alloy after heat treatment shows the precipitation of similar phases.

Acknowledgement

The authors would like to thank Profs. R. K. Mandal, S. Lele, Dr B. Mukherjee and Mr Vivek Kumar Pandey for stimulating discussion on various occasions.

References

[1] S. Ranganathan, Alloyed pleasures: multiatomic cocktails, Curr. Sci. 85 (2003) 1404–1406.
[2] B. Cantor, I.T.H. Chang, P. Knight, A.J.B. Vincent, Microstructural development in equiatomic multicomponent alloys, Mater. Sci. Eng. 375–377 (2004) 213–218.
[3] J.W. Yeh, S.K. Chen, S.J. Lin, J.Y. Gan, T.S. Chin, T.T. Shun, C.H. Tsau, S.Y. Chang, Nanostructured high-entropy alloys with multiple principal elements: novel alloy design concepts and outcomes, Adv. Eng. Mater. 6 (2004) 299–303.
[4] N.K. Mukhopadhyay, High entropy alloys: a renaissance in physical metallurgy, Curr. Sci. 109 (2015) 665–667.
[5] S.H. Joo, H. Kato, M.J. Jang, J. Moon, E.B. Kim, S.-J. Hong, H.S. Kim, Structure and properties of ultrafine-grained CoCrFeMnNi high-entropy alloys produced by mechanical alloying and spark plasma sintering, J. Alloys Compd. 698 (2017) 591–604.
[6] B. Schuh, F. Mendez-Martin, B. Volker, E.P. George, H. Clemens, R. Pippan, A. Hohenwarter, Mechanical properties, microstructure and thermal stability of a nanocrystalline CoCrFeMnNi high-entropy alloy after severe plastic deformation, Acta Mater. 96 (2015) 258–268.
[7] Y.P. Wang, B.S. Li, M.X. Ren, C. Yang, H.Z. Fu, Microstructure and compressive properties of AlCrFeCoNi high entropy alloy, Mater. Sci. Eng. 491 (2008) 154–158.
[8] S. Mohanty, T.N. Maity, S. Mukhopadhyay, S. Sarkar, N.P. Gurao, S. Bhowmick,

K. Biswas, Powder metallurgical processing of equiatomic AlCoCrFeNi high entropy alloy: microstructure and mechanical properties, Mater. Sci. Eng. A 679 (2017) 299–313.
[9] C. Wang, W. Ji, Z. Fu, Mechanical alloying and spark plasma sintering of CoCrFeNiMnAl high-entropy alloy, Adv. Powder Technol. 25 (2014) 1334–1338.
[10] W. Ji, Z. Fu, W. Wang, H. Wang, J. Zhang, Y. Wang, F. Zhang, Mechanical alloying synthesis and spark plasma sintering consolidation of CoCrFeNiAl high-entropy alloy, J. Alloys Compd. 589 (2014) 61–66.
[11] I. Moravcik, J. Cizek, P. Gavendova, S. Sheikh, S. Guo, I. Dlouhy, Effect of heat treatment on microstructure and mechanical properties of spark plasma sintered $AlCoCrFeNiTi_{0.5}$ high entropy alloy, Mater. Lett. 174 (2016) 53–56.
[12] Z. Cai, G. Jin, X. Cui, Y. Li, Y. Fan, J. Song, Experimental and simulated data about microstructure and phase composition of a NiCrCoTiV high-entropy alloy prepared by vacuum hot-pressing sintering, Vacuum 124 (2016) 5–10.
[13] S. Varalakshmi, M. Kamaraj, B.S. Murty, Synthesis and characterization of nanocrystalline AlFeTiCrZnCu high entropy solid solution by mechanical alloying, J. Alloys Compd. 460 (2008) 253–257.
[14] Y.L. Chen, Y.H. Hu, C.A. Hsieh, J.W. Yeh, S.K. Chen, Competition between elements during mechanical alloying in an octonary multi-principal-element alloy system, J. Alloys Compd. 481 (2009) 768–775.
[15] W. Chen, Z. Fu, S. Fang, H. Xiao, D. Zhu, Alloying behaviour, microstructure and mechanical properties in a $FeNiCrCo_{0.3}Al_{0.7}$ high entropy alloy, Mater. Des. 51 (2013) 854–860.
[16] S. Praveen, B.S. Murty, R.S. Kottada, Alloying behaviour in multi-component AlCoCrCuFe and NiCoCrCuFe high entropy alloys, Mater. Sci. Eng. 534 (2012) 83–89.
[17] Z. Fu, W. Chen, Z. Chen, H. Wen, E.J. Lavernia, Influence of Ti addition and sintering method on microstructure and mechanical behaviour of a medium-entropy $Al_{0.6}CoNiFe$ alloy, Mater. Sci. Eng. 619 (2014) 137–145.
[18] A. Upadhyaya, S.K. Tiwari, P. Mishra, Microwave sintering of W-Ni-Fe alloy, Scr. Mater. 56 (2007) 5–8.
[19] M. Oghbaei, O. Mirzaee, Microwave versus conventional sintering: a review of fundamentals, advantages and applications, J. Alloys Compd. 494 (2010) 175–189.
[20] P. Veronesi, E. Colombini, R. Rosa, C. Leonelli, F. Rosi, Microwave assisted synthesis of Si-modified $Mn25Fe_xNi25Cu_{(50-x)}$ high entropy alloys, Mater. Lett. 162 (2016) 277–280.
[21] R. Sriharitha, B.S. Murty, R.S. Kottada, Alloying, thermal stability strengthening in spark plasma sintered AlCoCrCuFeNi high entropy alloys, J. Alloys Compd. 583 (2014) 419–426.
[22] W.R. Wang, W.L. Wang, J.W. Yeh, Phases, microstructure and mechanical properties of AlxCoCrFeNi high-entropy alloys at elevated temperatures, J. Alloys Compd. 589 (2014) 143–152.
[23] R.L. Blaine, H.E. Kissinger, Homer Kissinger and the Kissinger equation, Thermochim. Acta 540 (2012) 1–6.
[24] T. Ozawa, A new method of analyzing thermogravimetric data, Bull. Chem. Soc. Jpn. 38 (1965) 1881–1886.
[25] B.Y. Zhang, Y.J. Zhou, J.P. Lin, G.L. Chen, P.K. Liaw, Solid-solution phase formation rules for multi-component alloys, Adv. Eng. Mater. (2008) 534–538.
[26] J. Basu, S. Ranganathan, Glass forming ability and stability: ternary Cu bearing Ti, Zr, Hf alloys, Intermetallics 17 (2009) 128–135.
[27] X. Yang, Y. Zhang, Prediction of high-entropy stabilized solid-solution in multi-component alloys, Mater. Chem. Phys. 132 (2012) 233–238.
[28] A.R. Miedema, P.F. de Châtel, F.R. de Boer, Cohesion in alloys—fundamentals of a semi-empirical model, Physica B 100 (1980) 1–28.
[29] J. Basu, B.S. Murty, S. Ranganathan, Glass forming ability: Miedema approach to (Zr, Ti, Hf)-(Cu, Ni) binary and ternary alloys, J. Alloys Compd. 465 (2008) 163–172.
[30] S. Fang, W. Chen, Z. Fu, Microstructure and mechanical properties of twinned Al0.5CrFeNiCo0.3C0.2 high entropy alloy processed by mechanical alloying and spark plasma sintering, Sicong 54 (2014) 973–979.
[31] S. Praveen, J. Basu, S. Kashyap, K.G. Pradeep, R.S. Kottada, Thermal stability and grain boundary strengthening in ultrafine-grained CoCrFeNi high entropy alloy composite, Mater. Des. 134 (2017) 426–433.
[32] J. Basu, S. Ranganathan, Glass - forming ability and stability of ternary Ni-early transition metal (Ti/Zr/Hf) alloys, Acta Mater. 56 (2008) 1899–1907.
[33] A. Inoue, Stabilization of metallic supercooled liquid and bulk amorphous alloys, Acta Mater. 48 (2000) 279–306.